

# Spatial and temporal correlations of coherent optical pulses in the photon echo effect

S. O. Elyutin,<sup>1)</sup> S. M. Zakharov,<sup>1)</sup> V. A. Zuikov,<sup>2)</sup> É. A. Manykin,<sup>1)</sup> and V. V. Samartsev<sup>2)</sup>

*Engineering-Physics Institute, Moscow  
Physicotechnical Institute, Branch of the  
Academy of Sciences of the USSR, Kazan*

(Submitted 12 July 1984)

Zh. Eksp. Teor. Fiz. **88**, 401–416 (February 1985)

An investigation is reported of the reproduction of the spatial and temporal profiles of coherent optical pulses in the photon echo generated by multipulse excitation of a resonant medium. It is shown that direct and mirror reproduction is possible in the stimulated and reconstructed photon echo signals, depending on the position of the coding pulse in a sequence of exciting pulses. The spatial and temporal correlations of coherent optical pulses are supported by the results of an experimental study of the photon echo in a ruby crystal.

The optical (photon) echo effect first studied in a ruby crystal<sup>1</sup> is now being used effectively to study kinetic processes in solids and in gases. In most cases the effect is used to measure relaxation times in resonant media, which is why the effect is employed extensively in high- and ultrahigh-resolution spectroscopy.<sup>2</sup> A new trend is now developing in the form of optical-echo spectroscopy with complex temporal profiles.<sup>3</sup> Coherent phenomena in the interaction of light pulses with resonant media are characterized by the formation of signals with a complex temporal envelope, such as the radiation-locked, jagged, anomalous, and many-hump echo.<sup>4,5,6</sup> The anomalies in the temporal profile of the optical echo may be accompanied by the delay or advance of echo pulses,<sup>1,7</sup> and also by distortion of the response profile away from a resonance.<sup>8</sup> Under certain conditions the envelope of a two-pulse photon echo is correlated with the profile of the first exciting light pulse, and the profile of the primary photon echo is inverted in time relative to the first pulse.<sup>9–11</sup> This theoretical conclusion is in agreement with the results of experiments on coherent response of resonant media: in particular, experiments have revealed reproduction of the profile of a low-intensity second exciting light pulse in the stimulated photon echo signal.<sup>10,12</sup> Since in the stimulated echo case the interval between the second and third exciting pulses is limited to the longitudinal relaxation time  $T_1$  and since for some crystals this relaxation time may reach several minutes at low temperatures,<sup>13,14</sup> the effect is important in applications, such as optical memory cells and delay lines.

We must stress that partial or complete reconstruction of temporal profiles of the exciting pulses in the photon echo signal occurs in the case of inequivalent excitation of an inhomogeneous line when the area under the coding-pulse signal is small and its duration is greater than the reversible relaxation time. Under these conditions the Rabi oscillation frequency in an external field is less than the inhomogeneous broadening of a resonance line. In final analysis, these features of the formation of a coherent response of a resonant medium appear because irreversible relaxation processes do not destroy the phase memory of the medium in the available time. Consequently, the properties of the medium are non-

linear functions not of the intensity but of the amplitude and phase of the field during all the preceding moments in time. It is known that this can be used to store the spatial structure of the wavefront of radiation and to reconstruct it at a moment other than the application of a coding or reconstructing pulse.<sup>15,16</sup>

When a resonant medium is excited by three light pulses, a series of echo signals is created and among these the most important are the stimulated and reconstructed echo.<sup>17,18</sup> The method of multipulse excitation of echo signals provides extensive opportunities for the control of the parameters of coherent spontaneous radiation, so that it is of interest to consider the temporal and spatial features of the echo signals in this case.

One of the present authors<sup>19</sup> demonstrated back in 1968 that a three-pulse photon echo satisfies quite definite phase relationships: if  $\Phi_a$  ( $a = 1, 2, 3$ ) is the phase of the exciting optical pulses transmitted by a resonant medium, the phase of the photon echo is

$$\Phi = 2\Phi_3 - 2\Phi_2 + \Phi_1 \quad (1)$$

for the reconstructed echo and

$$\Phi = \Phi_3 - \Phi_2 + \Phi_1 \quad (2)$$

for the stimulated echo (the indices 1, 2, and 3 refer to three consecutive optical pulses).

The relationships (1) and (2) derived in Ref. 19 are completely independent of whether  $\Phi$  is constant in space or whether it is an arbitrary function of the coordinate  $\mathbf{R}$ . When the phase is a linear function, i.e., when  $\Phi = \mathbf{k} \cdot \mathbf{R}$ , the relationships (1) and (2) transform into similar conditions for the wave vectors of plane waves of the corresponding optical pulses (these are known as spatial phase-matching conditions). Several variants of spatial phase matching of the three-pulse photon echo, including the case of wavefront reversal,<sup>17</sup> were considered later.

Technical applications of the optical echo effects simplify greatly when the reversal technique is used in which a resonant medium is pulse-excited by a sequence of traveling and standing waves.<sup>20</sup> Spatial reversal of the direction of propagation and of the wavefront is possible in the three-

pulse excitation regime and in the case of excitation by traveling-wave pulses when the wave vectors of the second and third pulses are oppositely directed.<sup>17</sup>

We shall report theoretical and experimental investigations of the reproduction of the spatial and time profiles of coherent optical pulses in the photon-echo signals obtained as a result of triple excitation of the resonant medium. The relationships (1) and (2) will be derived for a more general case and the relationship of the spatial wave fronts (constant-phase surfaces) of the photon echo and exciting pulses to their time profiles (pulse envelopes) will be considered. It will be shown that the time correlations, like those studied earlier,<sup>9</sup> are closely connected to the correlations in space, and numerous features of these correlations will be established.

Solutions of equations for the density matrix will be used to obtain the temporal and spatial profiles of the stimulated, reconstructed, and two-pulse echo signals as a function of the configuration and spectrum of the coding signal. It will be shown that the spatial and temporal correlations of coherent optical pulses are governed by the following factors in the photon echo effect: 1) amplitudes of the external signals; 2) duration and wavefront shape of these signals, and also the order of application of the coding and reconstructing signals.

It will be shown that the theoretical predictions are in satisfactory agreement with the experimental results obtained for a ruby crystal.

It will be demonstrated that the theory developed below provides a unified explanation of a wide class of spatial and temporal correlations in coherent optical processes, which—in our opinion—is not only of general physical interest, but also of practical importance in dynamic holography, optical delay lines, and memory cells.

## 1. PRINCIPAL EQUATIONS AND INITIAL ASSUMPTIONS

We shall now consider the approximation of a constant field or an optically thin medium. This approximation means that the field generated in a medium is weaker than the field of external pulses. In the opposite limit when the reaction of the medium cannot be ignored, we have to apply either numerical or special analytic methods.<sup>21,22</sup> Moreover, we shall postulate that the populations of the levels in the absence of a field hardly relax during the time interval in question and the quantum coherence described by nondiagonal elements of the density matrix decays exponentially at a rate characterized by the relaxation time  $T_2$ . Finally, we shall assume that the spatial and temporal profiles of the coding pulses remain constant.

The state of a resonant impurity ion in a crystal will be described by the density matrix  $\hat{\rho}(t)$  which satisfies the equation

$$i\hbar \left( \frac{\partial}{\partial t} + \hat{\Gamma} \right) \hat{\rho} = \hat{H}_0 \hat{\rho} - \hat{\rho} \hat{H}_0 + \hat{V} \hat{\rho} - \hat{\rho} \hat{V}. \quad (3)$$

The unperturbed Hamiltonian for a two-level system is

$$\hat{H}_0 = -\hbar \omega_{10} \hat{S}_z, \quad (4)$$

where  $\hbar \omega_{10}$  is the energy interval between the resonating states  $|1\rangle$  and  $|0\rangle$ ;  $\hat{S}_z$  is the operator of the effective spin

$S = 1/2$ . The operator of the interaction with an electric field  $\mathbf{E}$  can be expressed in the following form in the dipole approximation:

$$\hat{V} = -\hat{\mathbf{d}}\mathbf{E}, \quad (5)$$

$$\hat{\mathbf{d}} = \hat{\mathbf{d}}_{01} \hat{S}_+ + \hat{\mathbf{d}}_{10} \hat{S}_-, \quad \hat{S}_\pm = \hat{S}_x \pm i\hat{S}_y. \quad (6)$$

The term  $\hat{\Gamma} \hat{\rho}$  on the right-hand side of Eq. (3) describes the irreversible relaxation processes:

$$\hat{\Gamma} \hat{\rho} = -\gamma (\rho_{01} \hat{S}_+ + \rho_{10} \hat{S}_-), \quad \gamma = 1/T_2. \quad (7)$$

Initially, an ion is in the ground state so that the initial condition for Eq. (3) will be selected in the form

$$\hat{\rho}_0 = 1/2 \hat{1} + \hat{S}_z. \quad (8)$$

We shall now assume that a series of coherent light pulses is transmitted by a crystal and the electric field  $\mathbf{E}$  of these crystals is given by the expression

$$\mathbf{E}_a(\mathbf{R}_j, t) = \text{Re} \{ \tilde{\mathcal{E}}_a(\mathbf{R}_j, t) \exp[i\varphi_a(\mathbf{n}_a, \mathbf{R}_j) - i\omega t + i\Phi_a] \}. \quad (9)$$

Here,  $R_j$  is the coordinate of the  $j$ th ion in a crystal;  $\tilde{\mathcal{E}}_a$  is a slowly varying field amplitude (real quantity);  $\varphi_a$  is the spatial part of the optical wave phase describing the wavefront shape;  $\omega$  is the frequency of the field which is close to the frequency  $\omega_{10}$  of a transition in the resonating impurity;  $\mathbf{n}_a$  is the normal to the wavefront envelope;  $\Phi_a$  is the arbitrary initial phase;  $a = 1, 2, 3$  and it labels the sequence of pulses.

If the field of Eq. (9) is constant, a solution of Eq. (3) can be used to calculate the induced dielectric polarization of the medium at a point  $\mathbf{R}$  from the formula

$$\mathbf{P} = \sum_j \text{Sp} \{ \hat{\rho}(\mathbf{R}_j) \hat{\mathbf{d}} \} \delta(\mathbf{R} - \mathbf{R}_j), \quad (10)$$

where the summation is carried out over all the impurity ions. It should be noted that a deviation of the transition frequency  $\omega_{10}$  from a certain average value  $\omega_0$  results in an inhomogeneous broadening of a spectral line. In this case the summation in Eq. (10) can be replaced by integration over the spectrum of the  $g(\omega_{10} - \omega)$  line:

$$\mathbf{P} = N_0 \int d\omega_{10} g(\omega_{10} - \omega) \text{Sp} \{ \hat{\rho}(\mathbf{R}) \hat{\mathbf{d}} \}, \quad (11)$$

where  $N_0$  is the impurity concentration and the function  $g(\omega)$  is normalized to unity.

If we calculate the macroscopic polarization  $\mathbf{P}$  of the medium, we can use the reduced Maxwell equation to find readily the amplitude and intensity of the electric field in a medium,<sup>17</sup> which we shall not give here since its actual form is irrelevant to our main conclusions.

## 2. SOLUTION OF THE EQUATION FOR THE DENSITY MATRIX

Equation (3) can be solved using the approximation of rotating waves. We shall introduce the operator

$$\hat{\Lambda} = -\omega \hat{S}_z, \quad (12)$$

and subject the sought-for matrix  $\hat{\rho}(t)$  to a unitary transformation

$$\tilde{\sigma}(t) = \exp[i\hat{\Lambda}(t - t_a)] \hat{\rho}(t) \exp[-i\hat{\Lambda}(t - t_a)], \quad (13)$$

where  $t_a$  are the moments of arrival of the external signal at the point with the coordinate  $\mathbf{R}$ .

Using Eq. (13), we find that Eq. (3) becomes

$$i\hbar \left( \frac{\partial}{\partial t} + \hat{\Gamma} \right) \hat{\sigma} = \hat{h}_0 \hat{\sigma} - \hat{\sigma} \hat{h}_0 + \hat{W} \hat{\sigma} - \hat{\sigma} \hat{W}, \quad (14)$$

where

$$\hat{h}_0 = \hat{H}_0 - \hbar \hat{\Delta} = -\hbar(\omega_{10} - \omega) \hat{S}_z,$$

$$\hat{W} = \exp[i\hat{\Delta}(t-t_a)] \hat{V}(t) \exp[-i\hat{\Delta}(t-t_a)]. \quad (15)$$

After averaging over time intervals  $(\mathcal{E}_a d / \hbar)^{-1} \gg t \gg \omega^{-1}$  [which implies neglect of rapidly oscillating terms in  $\hat{W}(t)$ ], we obtain

$$i\hbar \left( \frac{\partial}{\partial t} + \hat{\Gamma} \right) \hat{\sigma} = \hat{h}_0 \hat{\sigma} - \hat{\sigma} \hat{h}_0 + \hat{U} \hat{\sigma} - \hat{\sigma} \hat{U}, \quad (16)$$

where

$$\begin{aligned} \hat{U}(t) = & -^{1/2} d_{01} \vec{\mathcal{E}}_a \exp(-i\varphi_a + i\omega t - i\Phi_a) \hat{S}_+ \\ & -^{1/2} d_{10} \vec{\mathcal{E}}_a \exp(i\varphi_a - i\omega t + i\Phi_a) \hat{S}_-. \end{aligned} \quad (17)$$

We shall seek a solution of Eq. (16) for three characteristic cases: a strong field, zero external field, and a weak field.

### Strong external field

In this case we shall assume that the parameters of external pulses satisfy the inequalities

$$d\mathcal{E}_a \hbar^{-1} \gg T_2^*, \quad \delta_a < T_2^* \ll T_2, \quad (18)$$

where  $\delta_a$  is the pulse duration. Using the relationships in Eq. (18), we can ignore both inhomogeneous and homogeneous broadening compared with the Rabi splitting in the field of a strong short pulse. Then, Eq. (16) becomes

$$i\hbar \partial \hat{\sigma} / \partial t = \hat{U} \hat{\sigma} - \hat{\sigma} \hat{U}, \quad (19)$$

and its solution can be described by the formula

$$\hat{\rho}(t) = \exp(-i\hat{F}_a \Theta_a) \hat{\rho}(t_a) \exp(i\hat{F}_a \Theta_a), \quad (20)$$

where

$$\Theta_a = d\hbar^{-1} \int_{t_a}^t \mathcal{E}_a(t') dt', \quad (21)$$

$d$  is the modulus of the matrix element of a dipole transition, and

$$\begin{aligned} \hat{F}_a = & -^{1/2} \exp(-i\varphi_a - i\Phi_a + i\omega t_a) \hat{S}_+ \\ & -^{1/2} \exp(i\varphi_a + i\Phi_a - i\omega t_a) \hat{S}_-. \end{aligned} \quad (22)$$

Finally, the density matrix in a strong field becomes

$$\begin{aligned} \hat{\rho}(t) = & \exp[-i\hat{\Delta}(t-t_a)] \exp(-i\hat{F}_a \Theta_a) \hat{\rho}(t_a) \\ & \times \exp(i\hat{F}_a \Theta_a) \exp[i\hat{\Delta}(t-t_a)]. \end{aligned} \quad (23)$$

It should be noted that a solution of Eq. (16) for  $\delta_a \ll T_2$  can be obtained also allowing for the contributions to the echo signal of individual radiators within the limits of an inhomogeneous line, but in this case the exciting pulses must have exactly rectangular profiles.<sup>23</sup>

### Zero external field

In the absence of an external field, Eq. (16) simplifies to

$$i\hbar \left( \frac{\partial}{\partial t} + \hat{\Gamma} \right) \hat{\sigma}^{(0)} = \hat{h}_0 \hat{\sigma}^{(0)} - \hat{\sigma}^{(0)} \hat{h}_0. \quad (24)$$

A solution of Eq. (24) subject to an allowance for relaxation of the (7) type is

$$\begin{aligned} \hat{\sigma}^{(0)}(t, t_0) = & \sigma_{01}^{(0)}(t_0) \exp[i(\omega_{10} - \omega + i\gamma)(t - t_0)] \hat{S}_+ \\ & + \sigma_{10}^{(0)}(t_0) \exp[i(\omega - \omega_{10} + i\gamma)(t - t_0)] \hat{S}_- + [^{1/2} \hat{1} + n(t_0) \hat{S}_z], \end{aligned} \quad (25)$$

$$n = \sigma_{00}^{(0)} - \sigma_{11}^{(0)} = \rho_{00} - \rho_{11}, \quad (26)$$

where  $n(t)$  represents the inversion process.

### Weak external field

In this case we shall assume that the parameters of external pulses satisfy the inequalities

$$d\mathcal{E}_a \hbar^{-1} \ll T_2^*, \quad \delta_a > T_2^*, \quad \theta_a \equiv \Theta_a(\infty) < 1. \quad (27)$$

Then, the small quantity  $d\mathcal{E}_a [\hbar(\omega_{10} - \omega)]^{-1} \ll 1$ , where  $\omega_0$  is the central frequency of an inhomogeneous line, can be used as the parameter of a linear (with respect to the field) perturbation theory:

$$\hat{\sigma} = \hat{\sigma}^{(0)} + \hat{\sigma}^{(1)}. \quad (28)$$

Here,  $\hat{\sigma}^{(0)}$  is given by Eq. (25).

Substitution of Eq. (28) into Eq. (16) gives, in the first approximation,

$$i\hbar (\partial / \partial t + \hat{\Gamma}) \hat{\sigma}^{(1)} = \hat{U} \hat{\sigma}^{(0)}(t, t_0) - \hat{\sigma}^{(0)}(t, t_0) \hat{U} + \hat{h}_0 \hat{\sigma}^{(1)} - \hat{\sigma}^{(1)} \hat{h}_0. \quad (29)$$

We shall seek the solution of Eq. (29) in the form

$$\hat{\sigma}^{(1)}(t) = \frac{1}{\sqrt{2\pi}} \int_{-\infty}^{+\infty} e^{i\nu(t-t_0)} \{ \hat{\mu}(\nu) + \exp[i(\omega - \omega_{10} + i\gamma)] \hat{\eta}(\nu) \} d\nu, \quad (30)$$

where the matrices  $\hat{\lambda}(\nu)$  and  $\hat{\eta}(\nu)$  have, respectively, the anti-diagonal and diagonal forms. Substitution of the expansion (30) into Eq. (29) makes it possible to determine the form of these matrices after certain transformations:

$$\hat{\mu}(\nu) = \frac{1}{\hbar^2} \frac{\hbar \xi(\nu) - 2\hat{\sigma}}{\xi^2 - (\omega_{10} - \omega)^2} [ \hat{Q}(\nu), (^{1/2} \hat{1} + n(t_a) \hat{S}_z) ], \quad (31)$$

$$\hat{\eta}(\nu) = 2\pi \sigma_{10}(t_a) \frac{1}{\hbar} \frac{[ \hat{Q}(\nu), \hat{S}_- ]}{\nu + \omega - \omega_{10} + i\gamma} + \text{H.c.},$$

where

$$\hat{Q}(\nu) = \frac{1}{\sqrt{2\pi}} \int_0^\infty \hat{U}(t, \mathbf{R}_j) e^{-i\nu(t-t_a)} dt, \quad \xi(\nu) = i\gamma - \nu.$$

When Eq. (17) is used, the solution (30) becomes

$$\begin{aligned} \hat{\sigma}^{(1)} = & - \frac{n(t_a)}{2\hbar\sqrt{2\pi}} \exp(-i\varphi_a - i\Phi_a + i\omega t_a) \\ & \times \int_{-\infty}^{+\infty} \frac{d_{01} \vec{\mathcal{E}}_a(\nu) \exp(i\nu(t-t_a))}{\omega_{10} - \omega - \nu + i\gamma} \\ & \times d\nu \hat{S}_+ - \frac{n(t_a)}{2\hbar\sqrt{2\pi}} \exp(i\varphi_a + i\Phi_a - i\omega t_a) \\ & \times \int_{-\infty}^{+\infty} \frac{d_{10} \vec{\mathcal{E}}_a(\nu) \exp(i\nu(t-t_a))}{\omega_{10} - \omega + \nu - i\gamma} d\nu \hat{S}_-. \end{aligned}$$

$$+ \left[ \frac{\sqrt{2\pi}}{\hbar} \sigma_{10}(t_a) \exp(-i\varphi_a - i\Phi_a + i\omega t_a) \right. \\ \left. \times \int_{-\infty}^{+\infty} \frac{\vec{d}_{01} \vec{\mathcal{E}}_a(\nu) \exp[i(\nu + \omega - \delta_{10} + i\gamma)(t - t_a)] d\nu}{\nu + \omega - \omega_{10} + i\gamma} \hat{s}_z + \text{H.c.} \right], \quad (32)$$

where  $\vec{\mathcal{E}}_a(\nu)$  is the Fourier transform of the envelope of a light pulse with an index  $a$ , i.e.,

$$\vec{\mathcal{E}}_a(t) = \frac{1}{\sqrt{2\pi}} \int_{-\infty}^{+\infty} e^{i\nu(t-t_a)} \vec{\mathcal{E}}_a(\nu) d\nu.$$

The solution of Eq. (3) for the weak field case is

$$\hat{\rho}(t) = \exp[-i\hat{\Delta}(t-t_a)] \hat{\sigma} \exp[i\hat{\Delta}(t-t_a)], \quad (33)$$

where  $\hat{\sigma}$  is given by the relationship (32) and (25):  $\hat{\sigma} = \hat{\sigma}^{(0)} + \hat{\sigma}^{(1)}$ . Therefore, the solutions (23), (25), and (33) allow us to calculate the density matrix and, consequently, the induced polarization of the medium (11) for an arbitrary number of consecutively acting light pulses, the parameters of which are given by the inequalities (18) or (27).

### 3. INDUCED POLARIZATION

Let us assume that three light pulses are incident consecutively on a crystal at moments  $t_1$ ,  $t_2$ , and  $t_3$  and that their durations are  $\delta_1$ ,  $\delta_2$ , and  $\delta_3$ , respectively (Fig. 1). One of these pulses satisfies the conditions of Eq. (27) and has the specified profile (coding pulse). We shall assume that in the most general case all three pulses are spherical waves of the converging or diverging type with centers at the points characterized by the radius vectors  $\mathbf{R}_{01}$ ,  $\mathbf{R}_{02}$ , and  $\mathbf{R}_{03}$ , so that

$$\varphi_a(\mathbf{n}_a, \mathbf{R}_j) = \pm k_a |\mathbf{R}_j \pm \mathbf{n}_a \mathbf{R}_{0a}|.$$

Here, the upper and lower signs refer to diverging and converging spherical waves, respectively. Then, the moments of arrival of the fronts of the light waves at a point with the coordinate  $\mathbf{R}_j$  can be written as follows:

$$\omega t_1(\mathbf{R}_j) = \psi_1(\mathbf{R}_j, \mathbf{R}_{01}),$$

$$\omega t_2(\mathbf{R}_j) = \psi_2(\mathbf{R}_j, \mathbf{R}_{02}) + \tau_1 + \delta_1, \quad (34)$$

$$\omega t_3(\mathbf{R}_j) = \psi_3(\mathbf{R}_j, \mathbf{R}_{03}) + \tau_1 + \tau_2 + \delta_1 + \delta_2,$$

$$\psi_a(\mathbf{R}_j, \mathbf{R}_{0a}) = (-1)^{\alpha_a} (k_a |\mathbf{R}_j - \mathbf{R}_{0a}| - k R_{0a}),$$

where  $\tau_1$  and  $\tau_2$  are the time intervals between the pulses;  $\psi_2$  is the spatial phase factor;  $\alpha_a = 0$  corresponds to a diverging spherical wave and  $\alpha_a = 1$  to a converging wave;  $k = \omega/c$ .

Using the expressions given in Sec. 2, we can find the density matrix  $\hat{\rho}(t)$  and then calculate the dipole moment of the  $j$ th ion. Averaging of the expressions obtained in this way over an inhomogeneous line makes it possible to calculate the macroscopic polarization of the investigated medium. The problem of averaging over the frequencies of an inhomogeneous line subject to a weighting function of one kind or another can usually be completed only numerically. Analytic expressions can be obtained for a very small number of cases: a) pulses of rectangular shape; b) short pulses ( $d_p \ll T_2^*$ ); c) pulses with a spectrum which "burns out" only a very narrow packet of natural frequencies near the frequency of the external field. It should be pointed out that the last circumstance is particularly important from the point of view of precision of reproduction of the temporal profile of

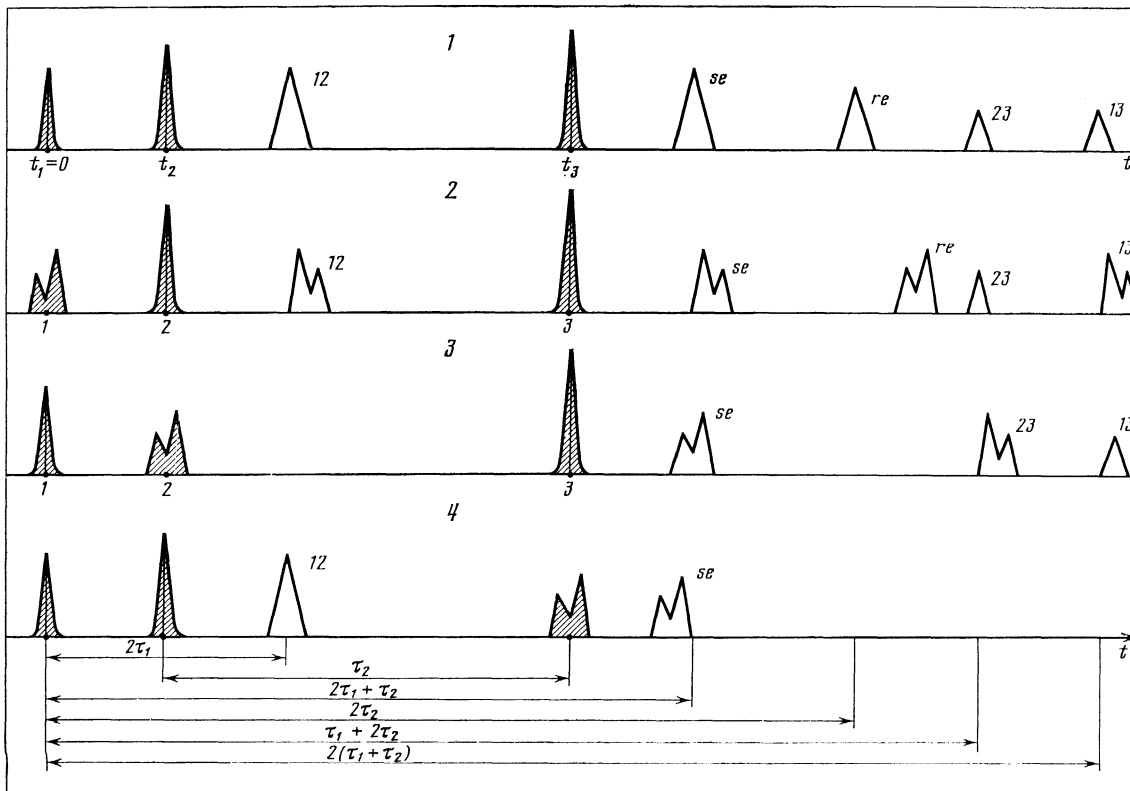


FIG. 1. Schematic representation of the appearance of coherent radiation of the photon-echo type as a result of excitation with three light pulses shown for four excitation regimes; here,  $t_a$  are the moments of application of the field;  $\tau_1$  and  $\tau_2$  are the time intervals between the exciting (shaded) pulses.

the photon echo pulses. For the sake of simplicity, we shall assume that the external field frequency is tuned to the center of an inhomogeneous line. The inaccuracy of the resonance setting becomes important only on excitation of a large part of the line and gives rise to beats between the external field and oscillations of the polarization of the medium.<sup>9</sup>

Calculations show that the macroscopic dipole moment contains eight terms that determine the properties of coherent spontaneous radiation. Three pulses appear simultaneously with the external pulses. The temporal profile and the characteristic features of the formation of such signals in the optical and rf frequency ranges have been considered in several earlier investigations,<sup>23,24</sup> so that we shall not discuss them here. The remaining five responses of the medium are the photon echo pulses: the echo of the first and second pulses (12), the echo of the first and third pulses (13) and of the second and third pulses (23), and the stimulated (*se*) and reconstructed (*re*) echo. Only these terms will be allowed for in the future. We shall simplify the formulas given below by assuming that the durations of the pulses other than the coding pulse are short compared with  $\tau_1$  and  $\tau_2$ , and also short compared with the duration with the coding pulse.

The final expression for the polarization at the moments of appearance of an echo pulse reads as follows:

$$\mathbf{P} = N_0 \mathbf{d} \sum_{b=1}^5 \operatorname{Re} \{ \mathcal{P}_b(\mathbf{R}, t) \exp [i\beta_b \psi_b(\mathbf{R}, \mathbf{R}_b) - i\omega_b t] \}, \quad (35)$$

$$\mathcal{P}_b(\mathbf{R}, t) = f_b G_b(t) \exp \{ -2\gamma(\tau_b + T_b(\mathbf{n}_b, \mathbf{R})) - i\Phi_b \}, \quad (36)$$

$$|\mathbf{R} - \mathbf{R}_b|^{-1},$$

where the index  $b$  has the values  $b = (12), (13), (23), (se), (re)$ ;  $\omega_b = \omega_0$  applies to the excitation regime 1 (Fig. 1) and to the echo pulses with the indices (23) (regime 3) and (13) (regime 2);  $\beta_b = \omega_0/\omega$  applies to all these cases, whereas for all other cases we have  $\beta_b = 1$ ,  $\omega_b = \omega$ . The vectors  $\mathbf{n}_b$  specify the direction of propagation of the echo signal wavefront and are governed by the familiar spatial phase-matching conditions for the coherent states of radiators and of the radiation field<sup>17</sup>:

$$\begin{aligned} \mathbf{n}_{12} &= 2\mathbf{n}_2 - \mathbf{n}_1, & \mathbf{n}_{13} &= 2\mathbf{n}_3 - \mathbf{n}_1, & \mathbf{n}_{23} &= 2\mathbf{n}_3 - \mathbf{n}_2, \\ \mathbf{n}_{se} &= \mathbf{n}_3 + \mathbf{n}_2 - \mathbf{n}_1, & \mathbf{n}_{re} &= 2\mathbf{n}_3 - 2\mathbf{n}_2 + \mathbf{n}_1, \end{aligned} \quad (37)$$

$\mathbf{R}_b$  is the radius vector of the center of a spherical echo wave. The parameters  $\tau_b$  specify the times of formation of the coherent response pulses deduced on condition that  $\tau_b = 0$ :

$$\begin{aligned} \tau_{12} &= t - \psi_{12}\omega^{-1} - 2\tau_1 - \delta_1 - \delta_2, \\ \tau_{13} &= t - \psi_{13}\omega^{-1} - 2(\tau_1 + \tau_2) - \delta_1 - \delta_2 - \delta_3, \\ \tau_{se} &= t - \psi_{se}\omega^{-1} - (2\tau_1 + \tau_2) - \delta_1 - \delta_2 - \delta_3, \\ \tau_{23} &= t - \psi_{23}\omega^{-1} - (2\tau_2 + \tau_1) - \delta_1 - \delta_2 - \delta_3, \\ \tau_{re} &= t - \psi_{re}\omega^{-1} - 2\tau_2 - \delta_1 - \delta_2 - \delta_3, \end{aligned} \quad (38)$$

where the phases  $\psi_b$  determine the spatial structure of the echo wavefront. The phases  $\psi_b$  are given by relationships similar to those in Eq. (37):

$$\begin{aligned} \psi_{12} &= 2\psi_2 - \psi_1, & \psi_{13} &= 2\psi_3 - \psi_1, & \psi_{23} &= 2\psi_3 - \psi_2, \\ \psi_{se} &= \psi_3 + \psi_2 - \psi_1, & \psi_{re} &= 2\psi_3 - 2\psi_2 + \psi_1. \end{aligned} \quad (39)$$

The parameters  $f_b$  characterizing the relationship between the amplitude of the photon echo pulses and the "areas"  $\theta_a$  under the excitation pulses are similar to those considered in Ref. 3. The initial phases  $\Phi_b$  are expressed in terms of the phases  $\Phi_a$  of the incident fields using the phase-matching conditions of the type given by Eq. (37) allowing for the phase advance during a coding pulse.

The geometric corrections  $T_b(\mathbf{n}_b, \mathbf{R})$  are expressed in terms of the phases  $\psi_a$  and in terms of the off-duty factor of the pulses  $\tau_{1,2}$  using the formulas

$$T_{12} = (\psi_2 - \psi_1)/\omega + \tau_1, \quad T_{13} = (\psi_3 - \psi_1)/\omega + \tau_1 + \tau_2,$$

$$T_{23} = (\psi_3 - \psi_2)/\omega + \tau_2, \quad T_{se} = (\psi_2 - \psi_1)/\omega + \tau_1,$$

$$T_{re} = (\psi_3 - \psi_2)/\omega + \tau_2.$$

The parameters  $G_b(t)$  describe the temporal profiles of the echo response pulses which are shown schematically, together with the moments of their appearance, in Fig. 1. The time in the expressions (35) and (36) is  $t > t_3(\mathbf{R})$  for all the terms with the exception of  $b = (12)$ , in which case we have  $t > t_2(\mathbf{R})$ .

#### 4. DISCUSSION OF THEORETICAL RESULTS

A remarkable property of the photon echo is the correlation between the temporal profiles of the coding and echo pulses. Transposition on the time axis of the strong and coding signals can be used to "read out" (reconstruct) the pulse profile in the forward and reverse directions (Fig. 1). The physical reason for this effect is the ability to establish conditions under which the stimulated photon echo signal is a linear function of the field of any of the three excitation light pulses. This is why in the conventional case of echo excitation and in the reconstructed photon echo only the first light pulse can act as the coding pulse. Otherwise, the echo response is of the second order of smallness with respect to  $\mathcal{E}_c$ .

The exponential factor in Eq. (36) describes the processes of irreversible relaxation of the polarization. It should be pointed out that the damping of the responses with the index *se* does not depend on the interval between the second and third pulses. This is due to the fact that the field of the second signal alters the relaxation time of quantum coherence (near-diagonal elements of the density matrix). The second pulse transfers part of the phase memory of the medium to the diagonal elements of the density matrix, i.e., to the population which decays at a rate described by the characteristic longitudinal relaxation time. In our calculations it was assumed that  $T_1 = \infty$ . For example, in the stimulated echo pulse in the regime 4 there is no irreversible relaxation at all.

The spatial correlations of the wavefronts of the excitation and echo pulses follow from the phase relationships (39) for the quantities  $\psi_a$  and it is assumed that  $R \ll R_0$  (or, in other words, that  $L \ll R_0$ , where  $L$  is the length of the sample). Then, the spatial part of Eq. (35) yields the universal expression for the wavefront of any type of echo:

$$P_{\text{echo}}(\mathbf{R}, \mathbf{n}_b) \propto \exp \left\{ i \frac{\omega}{c} |\mathbf{n}_b| \left[ \frac{r_b}{|r_b|} |\mathbf{R} + \mathbf{n}_b r_b| - |\mathbf{n}_b| r_b \right] \right\}, \quad (40)$$

where  $r_b$  is related to the parameters  $\lambda_a = (-1)^{\alpha_a} R_{0a}^{-1}$  by

conditions similar to those given by Eq. (39). The parameter  $|r_b| \neq 0$  in the  $R_{0a} < \infty$  case represents the radius of curvature of the photon echo wavefront. The radius vector  $\mathbf{R}_b$ , which determines the position of the "center" of the echo wave can be expressed in terms of  $r_b$  using  $\mathbf{R}_b = -r_b \mathbf{n}_b$ .

Clearly, the type of the spherical wave representing the photon echo (converging or diverging) can generally be determined accurately only for a given ratio of the radii of curvature  $R_{0a}$  of the wavefronts of the external pulses at the position of the investigated sample. The sign of the quantity  $r_b$  then governs the type of the spherical wave. However, there are situations where the type of the wave is determined uniquely only by the sequence of waves with different profiles, irrespective of the relationship between the quantities  $R_{0a}$ .

By way of example, we shall consider the phenomenon of simulated echo involving spherical waves with  $\alpha = \{1,0,0\}$ , i.e., involving a sequence of three waves: converging, diverging, and diverging. Then,

$$r_{se}^{-1} = R_{01}^{-1} + R_{02}^{-1} + R_{03}^{-1} > 0, \quad (41)$$

$$P_{se}(\mathbf{R}, \mathbf{n}_{se}) \propto \exp \left\{ i \frac{\omega}{c} |\mathbf{n}_{se}| [ |\mathbf{R} + \mathbf{n}_{se} r_{se}| - |\mathbf{n}_{se}| r_{se} ] \right\}.$$

Therefore, in this case the stimulated echo is a diverging spherical wave with  $\mathbf{R}_{se} = -\mathbf{n}_{se} r_{se}$ . However, the combination  $\alpha = \{0,1,1\}$  describes a converging wave of the stimulated photon echo with its center at the point defined by the radius vector  $\mathbf{R}_{se} = \mathbf{n}_{se} |r_{se}|$ . It is important to stress that going to the limit  $R_{0a} \rightarrow \infty$  in Eq. (40) allows us to consider the results of the interaction of a combination of pulses with spherical and plane wavefronts with a resonant medium. It should be pointed out that if  $R_{01}, R_{02}, R_{03} \rightarrow \infty$ , we find from Eq. (40) the traditional conditions for spatial phase matching of a three-pulse photon echo.<sup>17</sup> The results obtained for various sequences of plane and spherical waves are collected in Table I.

In Table I the coding pulse has a wavefront different from the wavefronts of the other two pulses. For example, in columns 1–3 the coding signal has a spherical wavefront, whereas in columns 4–6 it has a plane wavefront. The heading of each of the six columns describes the sequence of the pulses with different spatial configurations (planar or spherical); the row below the column headings identifies the type of the spherical excitation wave: the plus sign corresponds to a diverging wave, whereas the minus sign represents a con-

verging wave. The next four rows, i.e., the main part of the table below the headings, represents the results obtained for five photon echo pulses. The symbol 0 is used for a plane wave,  $\pm$  is used in the case when the type of spherical wave is not definite for reasons given above. A long dash in a row represents a weak echo signal which is of the second order of smallness compared with the coding pulse field.

First of all, we must stress that the results in Table I demonstrate the feasibility of using the photon echo effect for wavefront reversal of light pulses [echo pulses (12), (13), and *se* in column 1] if the coding pulse has a spherical front. However, the pulse with the index *re* reconstructs the coding signal front without a change in the sign of curvature.

When the coding pulse is a plane wave (columns 4–6 in Table I), it is possible to select converging and diverging lenses of suitable optical power so as to generate a spherical echo wave of the required type. Finally, it should be pointed out that the scheme shown in Fig. 1 and that given in Table I (columns 1–3) are identical with respect to the correlations of the temporal and spatial profiles of the coding and echo pulses.

## 5. EXPERIMENTAL OBSERVATION OF THE PROFILE CORRELATION EFFECT

The correlation of the temporal profile of optical coherent response pulses with the profile of certain excitation pulses was investigated experimentally using a ruby crystal with a trivalent chromium ion concentration amounting to 0.05 mass%. The temperature of this crystal was 1.7–2.2 K. The system was excited and the echo signals were generated employing the  ${}^4A_2 \rightarrow {}^2E(E)$  transition. Excitation was provided by pulses from a ruby laser in which the active element was kept at liquid nitrogen temperature. The duration of the excitation pulses was 6 nsec and the time interval between the pulses was varied from 20 to 120 nsec. A universal Carl Zeiss UFPS spectrometer was used in a study of the emission spectrum of the low-temperature laser.

The duration of the pulses at half-maximum was 6 nsec ( $\pm 16\%$ ), the energy was 0.03 J ( $\pm 15\%$ ), and the power was 500 kW ( $\pm 18\%$ ). The average width at half-maximum of the emission spectrum was 0.007 Å. This was over an order of magnitude less than the inhomogeneous width of the  $R_1$  line of ruby ( $\Delta\omega = 10^{10} \text{ sec}^{-1}$ ) cooled to a liquid helium temperature. The emission wavelength of the low-temperature laser was 6935 Å. The average instability of the spectral composition from pulse to pulse did not exceed  $\pm 16\%$ .

TABLE I. Types of spatial configurations of photon echo wavefronts for different combinations of exciting pulses.

Type of echo	Sequence of waves											
	1		2		3		4		5		6	
	Spher.-plane-plane	Plane-spher.-plane	Plane-plane-spher.	Plane-spher.-spher.	Spher.-plane-spher.	Spher.-spher.-plane						
	+	–	+	–	+	–	++	---	++	---	++	---
1–2	–	+	–	–	0	0	+	–	–	–	±	∓
1–3	–	+	0	0	–	–	±	–	±	∓	–	–
2–3	0	0	–	+	–	–	±	∓	–	±	–	–
<i>se</i>	–	+	+	–	+	–	+	–	±	∓	∓	∓
<i>re</i>	+	–	–	–	–	–	±	∓	–	–	–	–

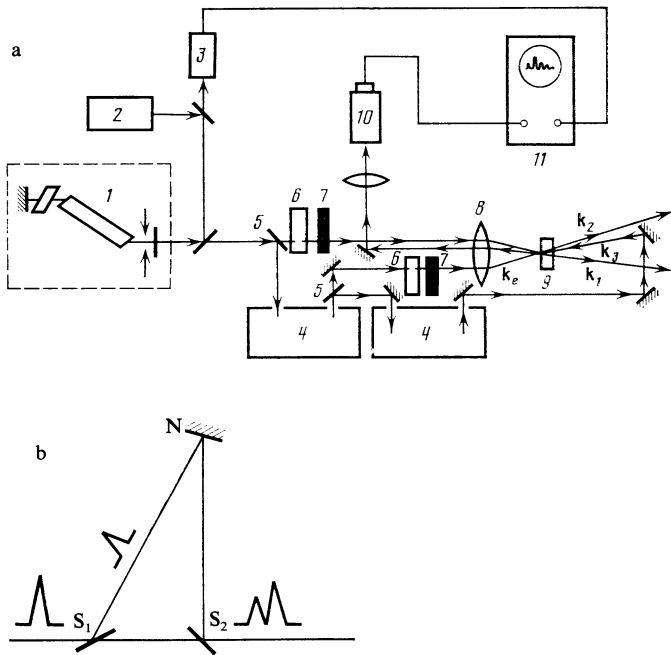


FIG. 2. a) Block diagram of the apparatus for investigating stimulated optical echo by determination of the temporal profiles of the coherent response and their correlations with the profiles of the exciting pulses: 1) low-temperature ruby laser; 2) helium-neon laser used for alignment; 3) synchronized photodetector (FÉK-15 coaxial photocell); 4) optical time-delay lines; 5) semi-transparent mirrors; 6) attachment for the formation of the temporal profile of a coding pulse; 7) set of optical filters for varying the intensity of the coding pulse; 8) lens; 9) sample; 10) ELU-FT photodetector; 11) I2-7 time interval meter. b) Attachment for varying the time profile of the coding pulse:  $S_1$  and  $S_2$  are semi-transparent mirrors and  $N$  is a nontransmitting mirror.

Therefore, the experimental situation corresponded to the case of partial excitation of an inhomogeneously broadened line by the narrow spectrum of the excitation pulses.

Signals were detected employing a synchronized FÉK-15 photodetector with a resolution of at least 2.7 nsec, which produced a signal that was applied to a time-interval meter of the I2-7 type. The apparatus made it possible to apply a static magnetic field up to 1500 G along the optic axis and this increased greatly the echo signal intensity. The correlation of the temporal profile was studied using the apparatus shown schematically in Fig. 2. A light pulse from a ruby laser 1 passed through a beam splitter. Part of the energy of this pulse was focused on a sample which was inside a helium cryostat. The other part of the energy was directed to a cascade of optical delay lines. After the delay the light pulses were focused on the sample by a system of lenses.

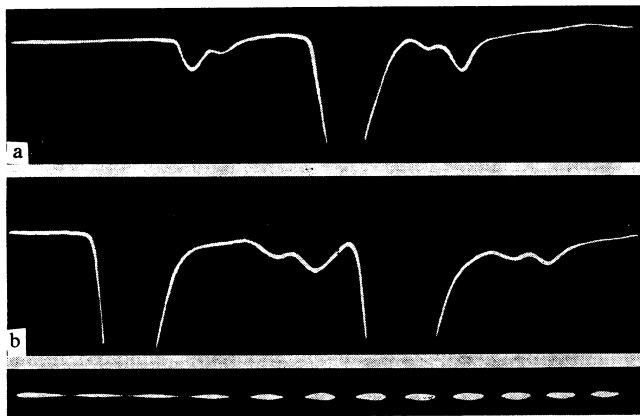


FIG. 3. Oscillograms illustrating the correlation effect in the case of a two-pulse photon echo (the coding pulse is shown first on the left) (a) and of a three-pulse stimulated echo (the coding pulse is shown on the left) (b). Power ratio  $W_c/W_s = 1/10$ ;  $W_s = 200$  kW. The timing marks are at intervals of 10 nsec.

The coding pulse was generated by a special construction, the basic construction of which is explained under the block diagram in Fig. 2. The shape of the coding pulse was set by two laser pulses of different amplitudes delayed relative to one another by 5–8 nsec. The resultant pulse should be asymmetric and it could be varied by altering the distance between mirrors in the attachment and the density of optical filters 7.

It was clear that we should use only one of the attachments 6, depending on whether the first or second pulse was the coding pulse. The apparatus shown in the block diagram could be used also to study the two-pulse excitation regime in which case it was necessary to remove the second delay line with the corresponding mirrors.

The spatial separation of the echo response pulses was ensured on the basis of the spatial phase-matching conditions. Figures 3 and 4 show oscillograms of the correlation effects in the case of conventional and stimulated echo under the experimental conditions described above. As already stressed in Sec. 2, reliable observation of the correlation of the temporal shape of the coding pulse and its echo response would require that the following conditions be satisfied:

$$d\mathcal{E}_c T_2^* \hbar^{-1} \gg 1, \quad d\mathcal{E}_s T_2^* \hbar^{-1} \ll 1, \quad \delta_c \gg T_2^*, \quad \theta_c \ll 1, \quad (42)$$

where  $\mathcal{E}_c$  is the amplitude of the coding pulse and  $\mathcal{E}_s$  is the amplitude of the stronger signals. Under the experimental conditions the inequalities of Eq. (42) could be rewritten in the form

$$W_c^{1/2} \hbar^{-1} d (8\pi/cS)^{1/2} T_2^* \gg 1, \quad (43)$$



FIG. 4. Oscillogram of the correlation of the profiles of the stimulated echo and coding pulse (first on the left).

$$W_c^{1/4} \hbar^{-1} d (8\pi/cS)^{1/2} T_2^* \ll 1, \quad (44)$$

$$\delta_c^{-1} T_2^* \ll 1, \quad (45)$$

$$W_c^{1/4} \hbar^{-1} d (8\pi/cS)^{1/2} \delta_c \ll 1, \quad (46)$$

where the transverse reversible relaxation time is  $T_2^* \approx 10^{-10}$  sec;  $d \approx 4.8$  cgs esu;  $c$  is the velocity of light;  $S$  is the cross-section area  $\approx 10^{-2}$  cm<sup>2</sup>;  $W$  is the power of the pulses.

For these parameters the experimental conditions of smallness of the coding signal field, compared with the scatter of the local electric fields at the positions of paramagnetic Cr<sup>3+</sup> ions given by Eq. (44) and the narrowness of its spectral line given by Eq. (45), are fully satisfied. On the other hand, the inequality (46) would be satisfied by shorter pulses. As shown in Ref. 9, in the case of coding pulses with areas above  $\pi/2$  the resultant many-hump structure could distort the correlation of the temporal profile of the excitation and echo pulses.

A correlation between the spatial form of the wavefront of the external radiation and the echo pulses<sup>25</sup> was observed experimentally in the reversed optical echo effect.<sup>26-28</sup> The experimental results agreed unambiguously with the data in Table I: wavefront reversal was experienced by the first pulse when the sequence of pulses was spherical-plane-plane. A special feature of the experiments was that the pulses with plane fronts were standing waves. In this case the photon echo pulse traveled counter to the direction of the wave vector of the first pulse and was independent of the direction of action of the standing wave (this made it possible to increase greatly the signal/noise ratio and to avoid the use of an optical switch).

Reversal of the wavefront of the photon echo signal in the ruby crystal was checked using apparatus whose block diagram is shown in Fig. 5.

A sample was subjected to two pulses, the first a traveling wave and the second a standing wave. The radiation of the first pulse was focused down to a point on a sample 8 using a lens 7 with a focal length  $R$ . The second pulse, delayed by an optical delay line 4, reached the same sample in the form of a plane wave. A standing wave was formed by a mirror 9 placed directly behind the sample. The photon echo signal counter to the direction of action of the first pulse was

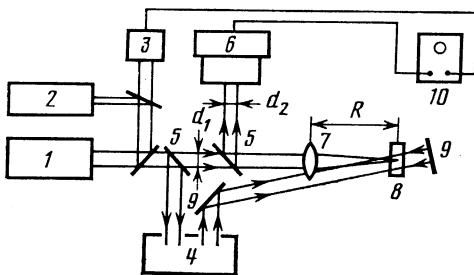


FIG. 5. Block diagram of the apparatus for investigating reversed photon echo signals: 1) low-temperature ruby laser; 2) laser used for alignment; 3) synchronizing photodetector; 4) optical delay line; 5) semitransparent mirrors; 6) recording photodetector; 7) spherical lens with a focal length  $R$ ; 8) investigated sample immersed in liquid helium; 9) mirrors; 10) time-interval meter;  $d_1$  and  $d_2$  are stops.

observed using a semi-transparent mirror 5. The divergence of this signal and, consequently, the radius of curvature of its wavefront could be determined from the size of an aperture in a stop  $d_2$ . An increase in the aperture of  $d_2$  to the size of the aperture in another stop  $d_1$  increased the echo intensity. A further increase in the aperture size ( $d_2 > d_1$ ) showed no significant increase in the photon echo signal. Consequently, the divergence of the echo signal radiation was equal to the angle of convergence of the traveling wave pulse, i.e., the wavefront of the photon echo signal was reversed relative to the front of the traveling wave.

## 6. CONCLUSIONS

Three-pulse excitation of a photon echo was found to provide more extensive opportunities for observing a correlation between the spatial envelope of the echo and the time profiles of the external fields, compared with the two-pulse echo. Excitation of a medium by three or more coherent light pulses not only increased the number of the echo signals from all possible pair combinations, but also resulted in the generation of stimulated and reconstructed echo specific to multipulse excitation. A characteristic feature of the correlation effect in the stimulated echo case was its dependence on the order of application of external pulses (direct or reverse order of profile reconstruction, shifts on the time scale), which was confirmed experimentally. These features of the stimulated echo were associated with a contribution to its generation of both nondiagonal and diagonal density matrix elements. The correlation of the temporal profiles of the external pulses with the echo pulses was linear in respect of the weak field of the coding signal. This ensured a single-valued storage of the frequency code in the background of an inhomogeneous line and then transformation of the radiation of excited "spin packets" into an echo pulse of specified profile.

The spatial features of the correlation effect were set by the phase-matching conditions since the type of the echo wave depended on the magnitude and sign of the curvature of the incident radiation wavefront. The spatial features of the three-pulse photon echo effect were manifested most clearly by a reversed optical echo and by simultaneous reversible changes in the time structure of the coherent spontaneous radiation pulses.

<sup>1</sup>Engineering-Physics Institute, Moscow.

<sup>2</sup>Physicotechnical Institute, Branch of the Academy of Sciences of the USSR, Kazan.

<sup>1</sup>I. D. Abella, N. A. Kurnit, and S. R. Hartmann, *Phys. Rev.* **141**, 391 (1966).

<sup>2</sup>V. V. Samartsev, *Zh. Prikl. Spektrosk.* **30**, 581 (1979); *Izv. Akad. Nauk SSSR Ser. Fiz.* **46**, 524 (1982).

<sup>3</sup>E. A. Manykin, S. O. Elyutin, S. M. Zakharov, V. N. Likhachev, and A. I. Maïmistov, *Izv. Akad. Nauk SSSR Ser. Fiz.* **46**, 538 (1982).

<sup>4</sup>P. F. Liao and S. R. Hartmann, *Phys. Lett. A* **44**, 361 (1973).

<sup>5</sup>U. Kh. Kopvillem, V. R. Nagibarov, V. A. Pirozhkov, V. V. Samartsev, and R. G. Usmanov, *Pis'ma Zh. Eksp. Teor. Fiz.* **20**, 139 (1974) [*JETP Lett.* **20**, 60 (1974)].

<sup>6</sup>R. L. Shoemaker, *Annu. Rev. Phys. Chem.* **30**, 239 (1979).

<sup>7</sup>V. V. Samartsev, R. G. Usmanov, G. M. Ershov, and B. Sh. Khamidulin, *Zh. Eksp. Teor. Fiz.* **74**, 1979 (1978) [*Sov. Phys. JETP* **47**, 1030 (1978)].

- <sup>8</sup>S. O. Elyutin, S. M. Zakharov, and É. A. Manykin, *Kvantovaya Elektron. (Moscow)* **3**, 357 (1976) [Sov. J. Quantum Electron. **6**, 189 (1976)].
- <sup>9</sup>S. O. Elyutin, S. M. Zakharov, and É. A. Manykin, *Zh. Eksp. Teor. Fiz.* **76**, 835 (1979) [Sov. Phys. JETP **49**, 421 (1979)].
- <sup>10</sup>V. A. Zuïkov, V. V. Samartsev, and R. G. Usmanov, *Pis'ma Zh. Eksp. Teor. Fiz.* **32**, 293 (1980) [JETP Lett. **32**, 270 (1980)].
- <sup>11</sup>N. W. Carlson, L. J. Rothberg, A. G. Yodh, W. R. Babbitt, and T. W. Mossberg, *Opt. Lett.* **8**, 483 (1983).
- <sup>12</sup>V. A. Zuïkov, V. V. Samartsev, and R. G. Usmanov, *Pis'ma Zh. Eksp. Teor. Fiz.* **31**, 654 (1980) [JETP Lett. **31**, 617 (1980)].
- <sup>13</sup>Y. C. Chen, K. P. Chiang, and S. R. Hartmann, *Opt. Commun.* **26**, 269 (1978).
- <sup>14</sup>J. B. W. Morsink and D. A. Wiersma, *Chem. Phys. Lett.* **65**, 105 (1979).
- <sup>15</sup>S. M. Zakharov and É. A. Manykin, *Opt. Spektrosk.* **45**, 390 (1978) [Opt. Spectrosc. (USSR) **45**, 218 (1978)].
- <sup>16</sup>E. I. Shtyrkov and V. V. Samartsev, *Phys. Status Solidi* **45**, 647 (1978).
- <sup>17</sup>S. M. Zakharov, É. A. Manykin, and É. V. Onishchenko, *Zh. Eksp. Teor. Fiz.* **59**, 1307 (1970) [Sov. Phys. JETP **32**, 714 (1971)].
- <sup>18</sup>N. A. Kurnit and S. R. Hartmann, *Bull. Am. Phys. Soc.* **11**, 112 (1966).
- <sup>19</sup>É. A. Manykin, *Pis'ma Zh. Eksp. Teor. Fiz.* **7**, 345 (1968) [JETP Lett. **7**, 269 (1968)].
- <sup>20</sup>V. A. Zuïkov, V. V. Samartsev, and E. A. Turiyanskiï, *Zh. Eksp. Teor. Fiz.* **81**, 653 (1981) [Sov. Phys. JETP **54**, 349 (1981)].
- <sup>21</sup>M. J. Ablowitz, D. J. Kaup, and A. C. Newell, *J. Math. Phys. (N.Y.)* **15**, 1852 (1974).
- <sup>22</sup>Yu. N. Karamzin, Preprint No. 74, Institute of Applied Mathematics, Academy of Sciences of the USSR, M., 1982.
- <sup>23</sup>S. M. Zakharov and É. A. Manykin, *Kvantovaya Elektron. (Moscow)* No. 2, 31 (1973) [Sov. J. Quantum Electron. **3**, 104 (1973)].
- <sup>24</sup>S. O. Elyutin, S. M. Zakharov, and É. A. Manykin, *Izv. Vyssh. Uchebn. Zaved. Radiofiz.* **22**, 1213 (1979).
- <sup>25</sup>C. V. Heer, *Phys. Rev. A* **7**, 1635 (1973).
- <sup>26</sup>V. A. Zuïkov, V. V. Samartsev, and R. G. Usmanov, *Izv. Akad. Nauk SSSR Ser. Fiz.* **46**, 600 (1982).
- <sup>27</sup>V. A. Zuïkov, V. V. Samartsev, and R. G. Usmanov, *V kn.: Prikladnye voprosy golografii (in: Applied Topics in Holography)*, Institute of Nuclear Physics, Leningrad, 1982, p. 175.
- <sup>28</sup>E. I. Shtyrkov, V. S. Lobkov, S. A. Moiseev, and N. G. Yarmukhamev, *Zh. Eksp. Teor. Fiz.* **81**, 1977 (1981) [Sov. Phys. JETP **54**, 1041 (1981)].

Translated by A. Tybulewicz